THE JOURNAL OF COMPARATIVE NEUROLOGY 507:1871-1878 (2008)

Different Types of Ganglion Cell Share a Synaptic Pattern

YING XU, VIREN VASUDEVA, NOGA VARDI, PETER STERLING, AND MICHAEL A. FREED*
Department of Neuroscience, University of Pennsylvania, Philadelphia, Pennsylvania 19104-6058

ABSTRACT

Retinal ganglion cells comprise about 10 morphological types that also differ functionally. To determine whether functional differences might arise partially from differences in excitatory input, we quantified the distributions of ribbon contacts to four mammalian ganglion cell types [brisk-transient (BT), brisk-sustained (BS), local edge (LE), directionally selective (DS)], comparing small vs. large and "sluggish" vs. "brisk." Cells in guinea pig retina were filled with fluorescent dye, immunostained for synaptic ribbons, and reconstructed with their ribbon contacts by confocal microscopy. False-positive contacts were corrected by performing the same analysis on processes that lack synapses: glial stalks and rod bipolar axons. All types shared a domed distribution of membrane that was well fit by a Gaussian function ($R^2 = 0.96 \pm 0.01$); they also shared a constant density of contacts on the dendritic membrane, both across each arbor and across cell types (19 ± 1 contacts/100 μm^2 membrane). However, the distributions of membrane across the retina differed markedly in width (BT > DS ≈ BS > LE) and peak density (BS > DS > LE > BT). Correspondingly, types differed in peak density of contacts (BS > DS ≈ LE > BT) and total number (BS ≈ BT > DS > LE). These differences between cell types in spatial extent and local concentration of membrane and synapses help to explain certain functional differences. J. Comp. Neurol. 507:1871-1878, 2008.

Indexing terms: retinal ganglion cell; dendrite; ribbon synapse; sluggish; brisk; guinea pig; membrane; microcircuit; retina; synaptic; visual; w-cell; x-cell; y-cell

Ganglion cells in mammalian retina comprise numerous types that differ strikingly in structure and function. Structural differences include extent of the dendritic field (narrow vs. broad) and density of branching (bushy vs. sparse). Functional differences include firing rate and information rate (sluggish vs. brisk) and trigger feature (local-edge vs. direction-of-motion). Furthermore, functionally distinct cell types are also structurally distinct. For example, the brisk-sustained (BS) cell has a narrow, bushy arbor, and the sluggish local-edge (LE) cell has a narrow, sparse arbor (Koch et al., 2004; Roska and Werblin, 2001; Troy and Shou, 2002).

We asked whether some functional differences might be explained simply by the differences in the distribution of dendritic membrane. For example, would the LE cell's sparse branching garner fewer excitatory synapses than the BS cell's dense branching? This would occur if the bipolar synapses were distributed to both types with equal density on the membrane. If this were generally true, then, simply by mapping a cell's membrane distribution, one could know the synaptic distribution.

Accordingly, we chose four cell types whose stylized dendritic patterns are agreed to correlate with their functions: BS, brisk-transient (BT), LE, and ON-OFF directionally selective (DS). The arbors were visualized by dye injection, then immunostained for synaptic ribbons (Jeon et al., 2002; Muresan et al., 1999), and finally reconstructed along with their ribbon contacts by confocal microscopy. Until recently, such quantitative mapping has required electron microscopy of serial sections and thus has been restricted to relatively few ganglion cells (see, e.g., Freed and Sterling, 1988; Kolb, 1979; McGuire et al.,

Grant sponsor: National Institutes of Health; Grant number: EY13333; Grant number: EY11105; Grant number: EY00828.

*Correspondence to: Michael Freed, 123 Anatomy/Chemistry Building, Department of Neuroscience, University of Pennsylvania School of Medicine, Philadelphia, PA 19104-6058. E-mail: michael@retina.anatomy.upenn.edu

Received 28 May 2007; Revised 31 August 2007; Accepted 19 December 2007

DOI 10.1002/cne.21644

Published online in Wiley InterScience (www.interscience.wiley.com).

1986; Weber et al., 1991). Here, confocal microscopy has allowed us to map bipolar synapses across a more substantial and diverse ganglion cell population (Jeon et al., 2002; Lin et al., 2000).

Materials and Methods

Preparation of retina and dye injection

After the animal received anesthesia (guinea pig, ~400 g) with ketamine, xylazine, and pentobarbital (100, 20, and 50 mg/kg), an eye was removed and the animal was killed by pentobarbital overdose, complying with guidelines of University of Pennsylvania and National Institutes of Health. As described elsewhere (Xu et al., 2005), the retina was mounted on a microscope stage and superfused with oxygenated Ames medium (34–36°C). Ganglion cells from the visual streak were injected with Lucifer yellow (Molecular Probes, Eugene, OR). The retina was fixed in 4% paraformaldehyde in 0.1 M pH 7.4 phosphate buffer (PB) for 30 minutes and stored in buffer at 4°C.

Immunocytochemistry

The retina was preincubated in buffered 10% goat serum, 5% sucrose, 0.01% sodium azide, and 0.5% Triton X-100 and then in primary antibody, mouse antikinesin (1:50), for 4 days at room temperature, later adding rabbit anti-Lucifer yellow (1:500; Invitrogen, Carlsbad, CA) for another 12 hours. Tissue was washed, incubated in secondary antibodies (goat anti-rabbit FITC, 1:100; and goat anti-mouse Cy3, 1:300; Jackson Immunoresearch Laboratories, West Grove, PA), then washed and coverslipped in Vectashield. Omitting primary antibodies revealed no staining. The monoclonal antibody against kinesin (clone K2.4) was generated in mouse against kinesin II purified from unfertilized sea urchin egg cytosol and was purchased from Covance (Princeton, NY; catalogue No. MMS-198P). This antibody, when applied to Western blots of mammalian retina, stains a double band at 85 kD (rat: Muresan et al., 1999). This antibody stains synaptic ribbons in mammalian retina (rat: Muresan et al., 1999; mouse: tom Dieck et al., 2005; rabbit: Jeong et al., 2006; Kwon et al., 2007; monkey: Jusuf et al., 2006). The polyclonal antibody against vimentin (diluted 1:2,000) was raised against human C-terminus amino acids 438–459 and was a gift from Virginia Lee (University of Pennsylvania). This antibody marks Müller cells in mammalian retina (Haverkamp and Wässle, 2000; Robinson and Dreher, 1990; Zhang et al., 2007). The polyclonal antibody against phosphokinase C (diluted 1:1,000) was raised in rabbit against the C-terminus region of the rat protein and was purchased from Sigma (St. Louis, MO; catalogue No. P 4334). This antibody marks retinal rod bipolar cells in a variety of species (Singer et al., 2004; Zhang et al., 2006).

Confocal microscopy

Ganglion cells were sectioned optically (0.2–0.5 μm steps) in a confocal microscope using a krypton/argon laser (488, FITC; 568 nm, Cy3). High magnification images (1,024 × 1,024 pixels) were photographed with a ×100, 1.4-NA oil objective, covering 50 × 50 μm with a confocal microscope (Leica Microsystems, Wetzlar, Germany). After averaging with a 3 × 3 median filter, objects were identified by watershed segmentation, a method that finds regions of pixels whose intensity values form a smooth gradient toward a common minimum (Vincent and Soille, 1991) and then were reconstructed in 3-D by using Volocity software (Improvision, Coventry, England). Dendritic membrane area was estimated by the marching cube algorithm for finding a polygonal mesh representation of a surface (Lorensen and Cline, 1987). Wider coverage was obtained with a ×10, 0.3-NA objective (500 × 500 μm) or a ×40, 1.25-NA oil objective (250 × 250 μm). Spatial resolution and channel alignment were checked with 1-μm fluorescent spheres coverslipped in Vectashield. High-magnification stacks resolved 200–300 nm in X/Y and 500–600 nm in Z. For presentation, image contrast and brightness were adjusted in Photoshop 7.0 (Adobe Systems, San Jose, CA).

Results

Identifying ganglion cells

We selected the following cell types (see Fig. 4): BT [narrowly stratified, radiate dendrites, broad field (>350 μm)]; BS [diffusely stratified, densely branched, narrow field (~200 μm)]; LE [narrowly stratified, sparsely branched, narrow field (~200 μm)]; ON-OFF DS [bistratified, loopy dendrites, medium field (~250 μm)]. These morphologies have been characterized functionally in several species, including rabbit, cat, and guinea pig (see, e.g., Amthor et al., 1984; Peichl and Wässle, 1981; Rockhill et al., 2002; Vaney, 1994; Xu et al., 2005).

Identifying bipolar synapses

Immunostaining for kinesin stained both outer and inner plexiform layers (OPL and IPL, respectively) in a pattern identical to that obtained in other species with the same antibody (Fig. 1A; rat: Muresan et al., 1999, mouse: tom Dieck et al., 2005, rabbit: Jeong et al., 2006; Kwon et al., 2007, monkey: Jusuf et al., 2006). In the outer plexiform layer, bright crescentic structures had the same shape, location, and distribution density as rod ribbons observed by electron microscopy and with other antibodies (Haverkamp et al., 2000). Clustered smaller structures had the same shape and distribution as cone ribbons observed by these other methods (Fig. 1B). In the inner plexiform layer, bright "puncta" (0.5–0.7 μm diameter) had the same size and distribution density as ribbons in bipolar cells of all types. The largest puncta in sublamina 5, corresponding to the location of rod bipolar axon terminals that are known to have the largest ribbons (Fig. 1C). Thus, the puncta in the IPL corresponded to synaptic ribbons that mark the presynaptic active zones of bipolar cells. Naturally, some puncta colocalized with dendrites of a dye-injected ganglion cell (Fig. 2A). However, it was difficult to tell how many of these colocalized puncta represented synapses on the ganglion cell, because the puncta distributed densely (~400/1,000 μm^3 of IPL), and thus an optical section contained many puncta that lay near the dendrite but not in actual contact. Consequently, the first task was to find puncta that optically overlapped the dendrites and were thus possibly in contact.

Accordingly, for each punctum near a dendrite, we drew a line through its center perpendicular to the dendrite. For puncta in the same optical section as the dendrite, this line lay within the section; for puncta in a different optical section, the line was orthogonal to the sections. Along this line

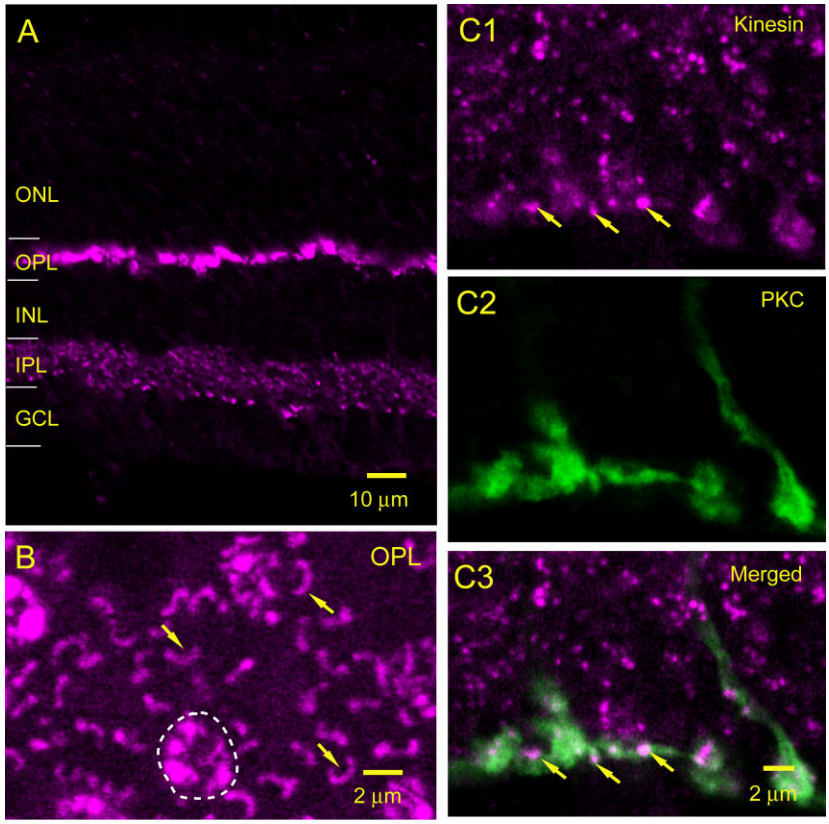

Fig. 1. Kinesin antibody stains synaptic ribbons in inner and outer plexiform layer. **A:** Immunostaining for kinesin (magenta) is restricted to the OPL and IPL, thus matching the distribution of synaptic ribbons. **B:** In OPL, kinesin puncta are either crescent shaped, thus matching synaptic ribbons in rod terminals (arrows), or in clusters, thus matching synaptic ribbons within cone terminals (encircled). **C:** In IPL, kinesin puncta (C1) colocalize with rod bipolar cells stained with phosphokinase C (C2; PKC, green); virtually all puncta near the ganglion cell layer (GCL) are within rod bipolar axon terminals, matching the concentration of synaptic ribbons (C3, arrows).

the intensity distributions of punctum and dendrite were plotted, calculating for each distribution the full width at half-maximum height. When the full widths at half height of both distributions overlapped by at least one pixel (~50 nm), the punctum was scored as a contact (Fig. 2B).

With this "manual" method, we scored ~1,300 contacts, but ultimately we had to count a much larger number (~39,000, as it turned out). To accelerate the counting, we applied an automated method to 3-D reconstructions of puncta and dendrites (see Materials and Methods). This automated method first eliminated voxels below a threshold intensity and cluster size; then, it found all puncta that overlapped a dendrite by at least one voxel. We adjusted the thresholds for intensity and cluster size until the automatic method provided the same number of contacts as the manual method (within 10%). Furthermore, two observers applying this method independently to the same neuron obtained nearly identical counts (25 vs. 23 puncta/100 μm^2 of dendritic membrane). The result for all ganglion cells was 28 ± 2 contacts/100 μm^2 of membrane (n = 14 cells; Fig. 3).

Both the manual and the automated methods were designed to find all puncta that appreciably overlapped the dendrites and were thus unlikely to miss any contacts (false negatives; see Discussion). However, because of blur in confocal images, both methods were liable to count puncta not in actual contact (false positives). To correct for false positives, we analyzed two types of process that are known not to receive ribbon synapses. First, we considered the Müller cell stalk where it traverses the IPL among ganglion cell dendrites (Fig. 2C). The stalk, immunostained for vimentin, was about as bright as the dye-filled ganglion cell dendrites. The manual and automated methods counting both found "contacts" on reconstructed Müller stalks, an average of 9.2 ± 1.1/100 μm^2 of membrane (n = 8 pieces of retina; Fig. 2E). Second, we considered rod bipolar axon stalks, which receive no ribbon contacts as they descend through the IPL's OFF stratum (Fig. 2D). These axons, immunostained for protein kinase C and comparable to the thicker ganglion cell dendrites, yielded 11.6 ± 1.6 contacts/100 μm^2 membrane (n = 6 pieces of retina). This was not statistically different from the Müller cell contact density (*t*-test, $P > 0.2$).

Because the Müller cell is more certain to lack contacts than the rod bipolar, we used its contact density as a correction factor to calculate the density of contacts on the ganglion cell:

$$\frac{\#\ \text{contacts}}{\text{membrane\_area}} = \frac{\#\ \text{puncta}}{\text{membrane\_area}} - \text{correction\_factor} \quad (1)$$

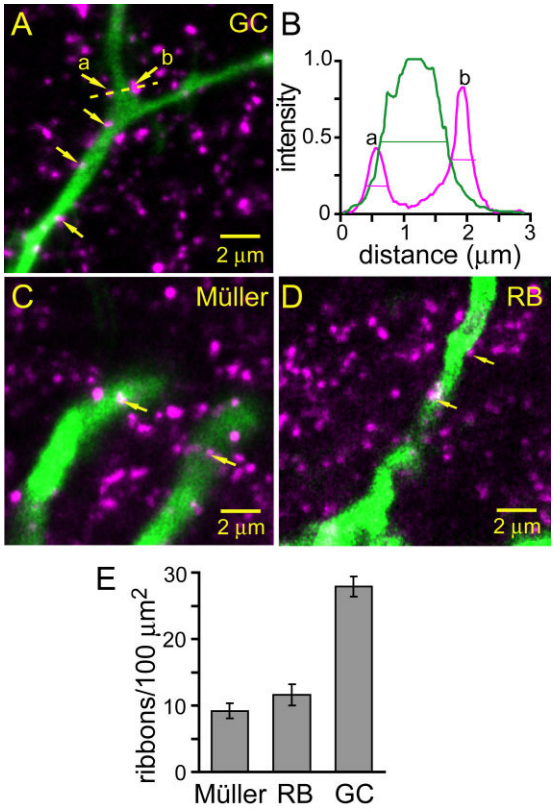

Fig. 2. Identifying contacts on ganglion cell dendrites. **A:** Ganglion cell dendrite (green) surrounded by puncta stained for kinesin. Some puncta overlap the dendrites (arrows). **B:** Plot shows pixel intensities along dashed line in A. Punctum a overlaps dendrite at half-width and is counted as a "contact"; punctum b does not overlap at half-width and is not counted. **C:** Müller cell processes (green) are overlapped by puncta (arrows) that cannot be contacts. **D:** Rod bipolar axons (green) are overlapped by puncta (arrows) unlikely to be contacts. **E:** Müller and rod bipolar processes show ~33% the membrane density of overlapping puncta on ganglion cell dendrites. Error bars indicate standard error of the mean.

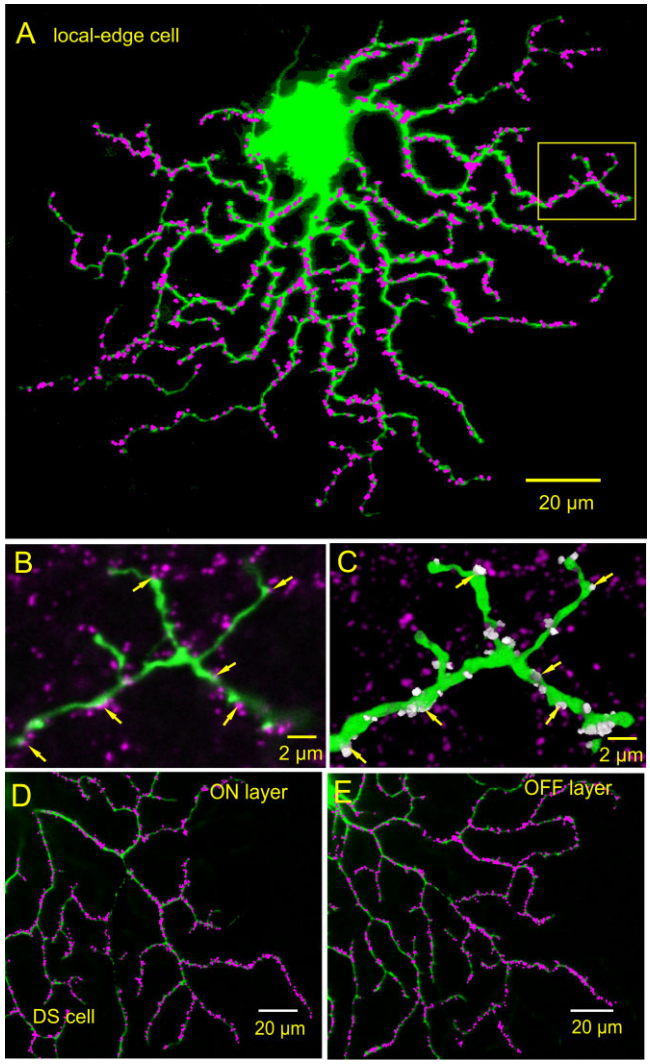

Fig. 3. Excitatory contacts distribute evenly across the dendritic arbor. **A:** Local-edge cell and its contacts reconstructed from multiple optical sections. **B:** Single section from A. Contacts to dendrite (some with arrows) were identified "manually." **C:** Same region reconstructed from multiple sections. All contacts identified by the automatic method are white. All contacts identified manually were also identified by the automatic method (arrows). Some contacts are from sections other than B. **D,E:** Reconstructed ON and OFF arbors of directionally selective cell with its contacts.

The overall result was 18 ± 2 contacts/100 µm^2 membrane for brisk cells and 21 ± 2/100 µm^2 for sluggish (no significant difference, *t*-test, $P = 0.49$). This method of confocal reconstruction cannot prove that any particular punctum actually contacts a particular dendrite; nevertheless, the synaptic densities obtained with this approach resemble closely what we have found by EM reconstructions of BT and BS cells (~20/100 µm^2; Freed and Sterling, 1988; Kier et al., 1995).

As further controls, we tested whether the number of contacts differed from the number expected by chance. First, we rotated a dendritic tree around an axis parallel to the retinal surface, thus "flipping" it. This significantly reduced the number of apparent contacts, indicating that they could not result solely from chance (35%, 12 stacks from four cells; Wilcoxon sign-rank test, $P < 0.0001$). Second, we mapped in this same plane the distribution of all puncta (including those not contacting a dendrite). The distribution departed significantly from a random clustering (nearest-neighbor distance analysis, $P < 0.001$; n = 29 sections from three cells; Boots and Getis, 1988).

Distribution of membrane across the dendritic arbor

For LE cells, about 10 high-magnification stacks covered the dendritic arbor completely (see Materials and Methods). From these stacks, we formed a 3-D reconstruction and calculated membrane area (n = 5 cells; Fig. 3A). Other types were too wide to cover fully at high magnification. Thus we covered at least two primary dendrites and their daughters with about 14 high-magnification stacks and from the resulting 3-D reconstructions extrapolated the full membrane area as follows (n = 9 cells). We collapsed the 3-D reconstructions to 2-D projections and calculated the ratio of projection area to membrane area.

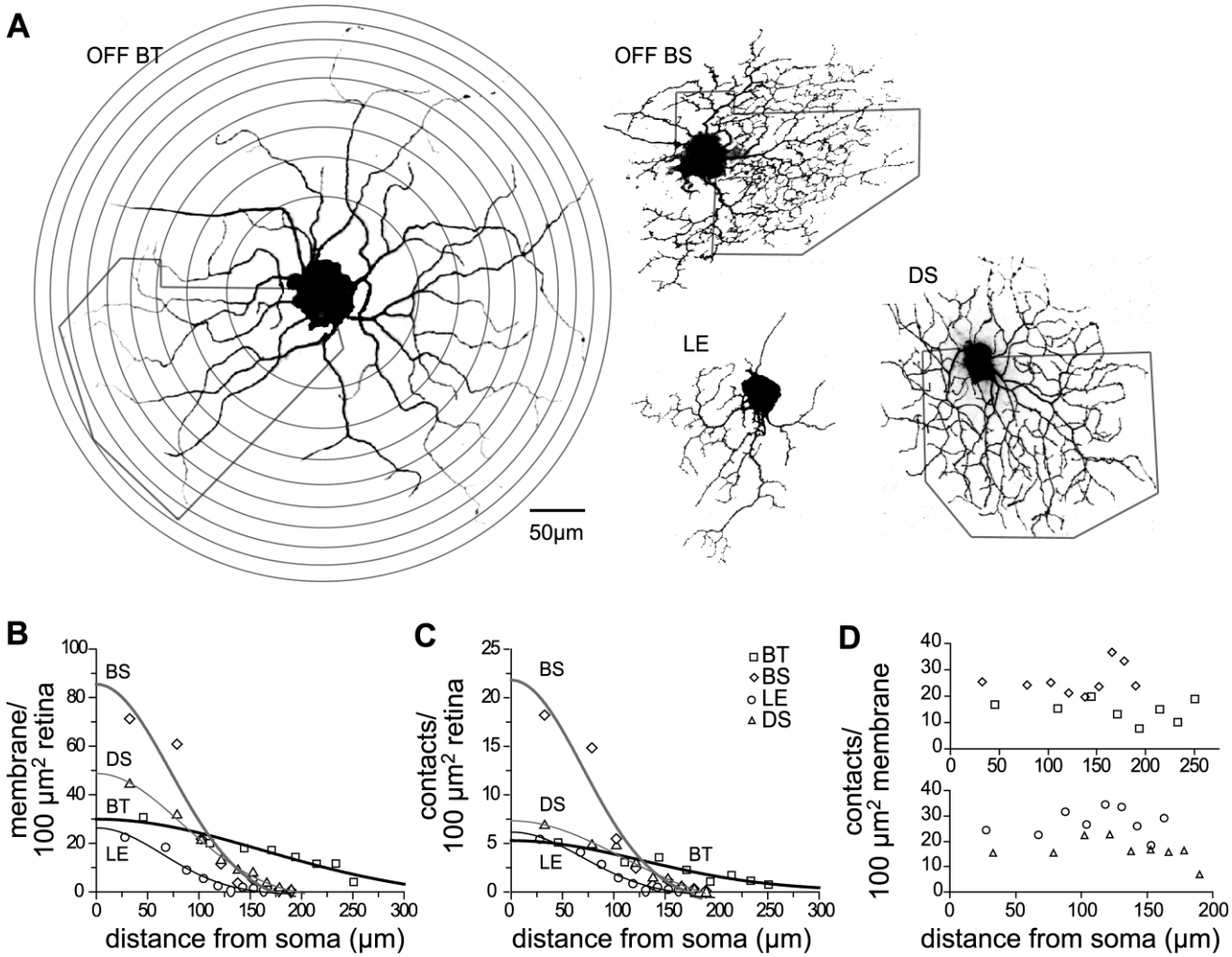

Fig. 4. Distributions of dendritic membrane and excitatory contacts. **A:** Each ganglion cell was divided into annuli of equal area (as shown for BT). Polygons indicate portions of each arbor that were reconstructed from high-magnification stacks: BT, 25%; BS, 45%; DS, 68%; LE, 100%. **B:** Membrane area/retinal area is well fit by a Gaussian distribution ($R^2 = 0.95 \pm 0.02$), but with a different standard deviation (σ) for each type: $\sigma_{BT} = 163$ μm; $\sigma_{DS} = 83$ μm; $\sigma_{BS} = 72$ μm; $\sigma_{LE} = 65$ μm). **C:** Contacts/retinal area (corrected for false positives) is also well fit by Gaussian distributions that match the membrane distributions in B. **D:** As a result of this match, the contacts/membrane area is even across the arbor.

To get the membrane area of any portion of the dendritic arbor, we multiplied the projection area—from low-magnification stacks that covered the entire dendritic arbor—by this ratio. Checking this method on two complete LE cells, we found the extrapolated membrane area of the entire arbor came within 5% of the same membrane area directly calculated from high-magnification stacks. We checked this by a second method: we measured for a BT cell the length and diameter of all dendrites, and, assuming cylindrical dendrites, calculated membrane area. The extrapolated membrane area of the entire arbor came within 5% of the same membrane area estimated by the first method.

For both small and large cells, we divided the dendritic field into concentric annuli of equal area (Fig. 4A) and calculated the membrane area for each annulus. All cells showed a domed distribution of membrane that was well fit by a Gaussian function ($R^2 = 0.96 \pm 0.01$; Figs. 4B, 5A):

$$G(x) = A\exp(-(X-X_0)^2/2\sigma^2) \quad (2)$$

The BT cell had the widest distribution ($\sigma = 137 \pm 9$ μm); the DS and BS cells were intermediate ($\sigma = 79 \pm 5$, 77 ± 5 μm), and the LE cell had the narrowest distribution ($\sigma = 63 \pm 4$ μm). Expressed as the peak amplitude of the Gaussian fit, the BS cell had the greatest concentration of membrane at the dendritic field center ($A = 105 \pm 15$ μm² membrane/100 μm² retina); the DS and LE cells were intermediate ($A = 69 \pm 10$ and 55 ± 11 μm² membrane/100 μm² retina, respectively), and the BT cell had the lowest density ($A = 30 \pm 4$ μm² membrane/100 μm² retina).

Density of contacts on membrane is constant across the dendritic arbor

For the LE cells, we calculated the number of contacts in each annulus directly from the high-magnification stacks.

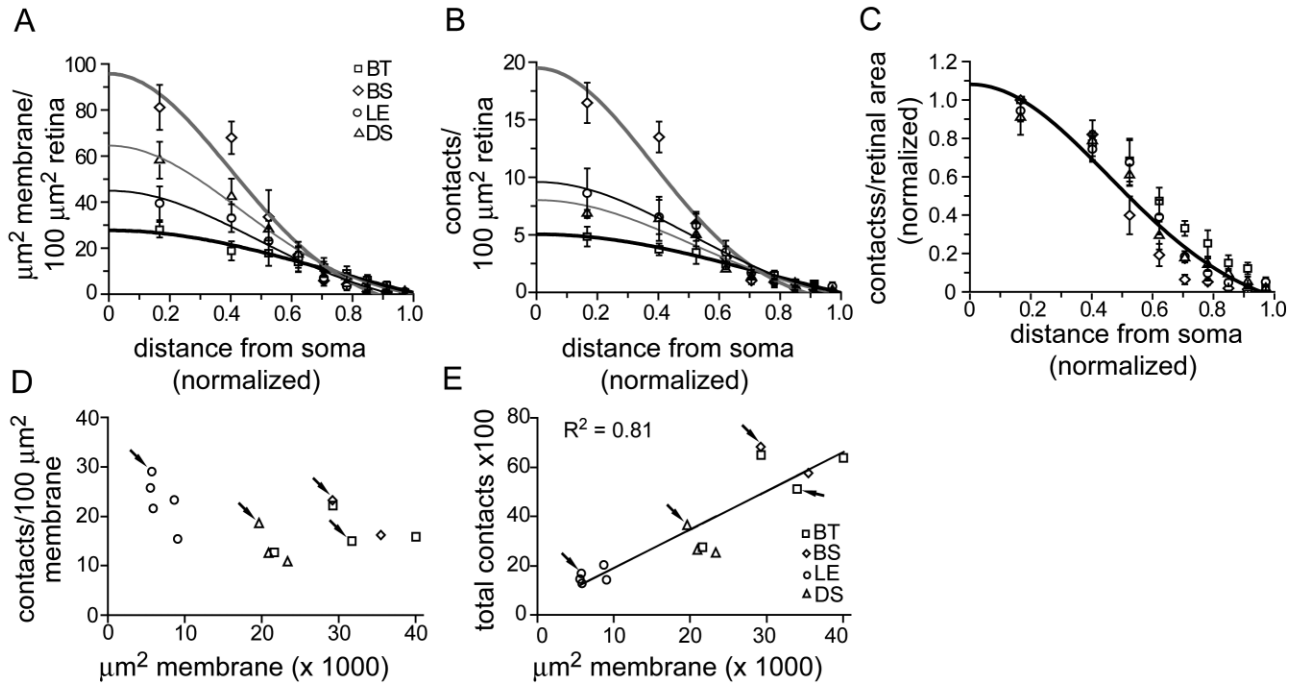

Fig. 5. Excitatory contacts to four cell types are proportional to membrane area. Graphs show averages for each cell type. **A:** Cell types differ in peak membrane area per retinal area: BS > DS > LE > BT. **B:** Cell types differ in peak density of contacts per retinal area: BS > DS ≈ LE > BT. **C:** When contacts per retinal area and distance from soma are both normalized, their distributions are fit by the same Gaussian function for all cell types ($R^2 = 0.95$). **D:** All cell types have similar number of contacts per membrane area, despite very different total membrane areas. Arrows indicate cells shown in Figure 4. **E:** Because contacts per membrane area are similar across cell types, total number of contacts correlated strongly with total membrane area ($R^2 = 0.81$).

For larger cells, we used the high-magnification stacks to calculate for each annulus the ratio of contacts to membrane area. Then to get the contact number for any annulus, we multiplied the membrane area within this annulus by this ratio.

The number of contacts was greatest near the soma and declined toward the periphery, thus creating a domed distribution that was well fit by a Gaussian function ($R^2 = 0.94 \pm 0.02$; Figs. 4C, 5B,C). The BT cell had the widest distribution ($\sigma = 150 \pm 22$ μm), the DS and BS cells had intermediate widths ($\sigma = 93 \pm 8$; 76 ± 6 μm), and LE cells were the narrowest ($\sigma = 59 \pm 8$ μm). As expressed by the peak amplitude of the Gaussian fit, the BS cell had the most contacts at the dendritic field center ($A = 21.2 \pm 1.7$/100 μm^2 retina), the LE and DS cells intermediate numbers (13.1 ± 3.6, 9.8 ± 1.3/100 μm^2 retina), and the BT cell the fewest (5.7 ± 1.2/100 μm^2 retina). We noted that the space constants for the distributions of membrane and contacts were similar, suggesting that contact density on the membrane was even throughout the arbor. In confirmation, the contact density on the membrane showed no trend from center to periphery of the arbor (Fig. 4D) and varied less than did membrane density: coefficient of variation (CV) was 0.33 ± 0.04 for contact density and 1.00 ± 0.07 for membrane density.

Density of contacts on membrane is constant across cell types

For each cell, we calculated the total number of contacts and the membrane area. These two measures were well correlated ($R^2 = 0.81$; Fig. 5E), a clear indication that contact density on the membrane was relatively constant across cell types (Fig. 5D). Thus ganglion LE cells with the least membrane area collected about 1,400 ribbon contacts, whereas ON-OFF DS cells with intermediate amounts of membrane collected about 3,000 contacts, and brisk types, with the greatest membrane area, collected nearly 6,000 contacts. BS cells had narrower dendritic fields than BT cells but, because of their denser local branching, had about the same membrane area as BT cells and thus similar numbers of contacts.

Discussion

Accuracy of optical method for identifying synapses

We mapped manually about 1,300 ribbon contacts and then used an automated procedure to map an additional 39,000 contacts onto 14 ganglion cells comprising four types. This exceeds by more than an order of magnitude all the synapses mapped by EM reconstructions from our laboratory over 20 years. Thus, although reconstructing synapse distributions by confocal microscopy requires considerable effort and care, it provides new information on a scale that EM cannot yet match, but is the method sufficiently accurate for its intended purpose?

False-negative errors—failing to count synapses on the dendrite—are unlikely because apparently every ribbon is stained. We infer that every ribbon is stained because

puncta distribute evenly through the full depth of the IPL, indicating that antibody penetration was complete. Also, we have used this same antibody to count ribbons in rod bipolar terminals and found that the numbers match EM reconstructions of that cell type (Singer et al., 2004). Furthermore, every ribbon close enough to contact a dendrite will be seen as a punctum that overlaps it and will be counted: a ribbon floats 30–40 nm from the membrane, the membrane is about 8 nm thick, and the synaptic cleft 20 nm wide, so the ribbon is at most 70 nm from the dendrite (Sterling and Matthews, 2005). Thus, because of blurring (~300 nm resolution of optical sections), the punctum will partially overlap the dendritic membrane.

The major source of inaccuracy in the optical method is false-positive errors resulting from blurring, counting puncta that are close to the dendrite but do not actually contact it. Thus we measured the density of puncta on cells that have no synaptic contacts (9.2 ± 1.1/100 μm^2); this we assumed was equal to the density of puncta on the ganglion cell dendrite that were distant from the dendrites but that appeared to overlap because of blurring. The density of all overlapping puncta on the ganglion cell dendrites averaged 27.9 ± 1.5/100 μm^2, so this indicated a false-positive rate of about 33%. The remaining puncta (true positives), at a density of approximately 19 ± 1 contacts/100 μm^2, were apposite to the dendrites and thus were actual synaptic contacts.

Another control, flipping the dendritic arbor, was able to demonstrate a statistically significant geometric relationship between ganglion cell dendrites and puncta. However, after flipping, about 65% of puncta remained suggesting a false-positive rate higher than the 33% derived from the Müller and rod bipolar cell controls. This is to be expected from the following test case. Consider the case if there were no false positives. Then, in order for the percentage of overlapping puncta remaining after flipping to equal the false-positive rate, there should be no remaining puncta, yet some puncta will inevitably overlap the ganglion cell's new position by chance. Thus the number of remaining overlapping puncta will exceed the false-positive rate.

Shared pattern of excitatory input

We conclude that different types of ganglion cell share two features that determine the distribution of excitatory synapses across their arbors. First, dendritic membrane distributes as a domed function that is well fit by a Gaussian (Fig. 5A). This point was established previously for brisk ganglion cells in cat retina (Freed et al., 1992; Kier et al., 1995) but is shown here to hold true also for sluggish types. Second, bipolar synapses distribute in proportion to available dendritic membrane (Fig. 5C,D). This emerges as a general principle of ganglion cell design. Because the density of contacts on the dendritic membrane holds across types and even across species (~20/100 μm^2 membrane), one can now estimate the number and distribution of ribbon contacts to any ganglion cell simply from its membrane area. An apparent exception is primate fovea, where densities of bipolar synapses on the membrane are somewhat higher (Calkins and Sterling, 2007).

Functional differences from variations on the shared pattern

Despite the shared pattern, cell types differ in the local concentration and extent of dendritic membrane. This, of course, is what allows one to recognize morphological types. Now we can suggest that these distributions of membrane, by setting characteristic concentrations and numbers of synapses, set sensitivity to visual stimuli. Excitatory synapses are the predominant source of signal and noise at the ganglion cell's input; because their release is a Poisson process, the number of synapses (n) would set signal-to-noise ratio in proportion to $\sqrt{n}$ (Freed, 2000). Thus, the BS cell concentrates its membrane about threefold more densely over the retina than the BT cell (Fig. 6; Kier et al., 1995) and is correspondingly more sensitive to a small spot on the receptive field center (Linsenmeier et al., 1982). The BS cell also concentrates its membrane more densely than the LE cell, collecting about fourfold more synapses over a similar-sized dendritic arbor. Correspondingly, the BS cell is more sensitive to a high-contrast spot that covers the receptive field (Xu et al., 2005). In general, the "sluggish" types (Troy and Shou, 2002), which may provide less total membrane and receive fewer excitatory synapses, fire at lower rates than brisk types and transmit less information (Koch et al., 2006).

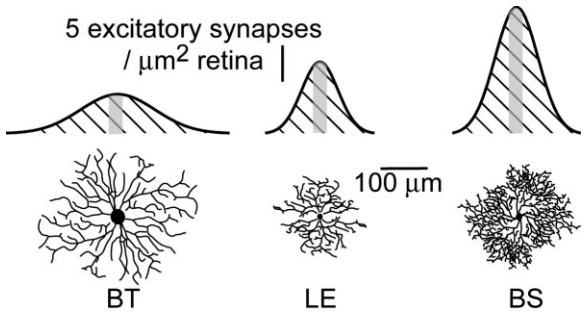

Fig. 6. Variations on a shared synaptic pattern lead to functional differences. A brisk-transient cell distributes membrane (and excitatory contacts) as a broad, shallow Gaussian, so a small spot activates few synapses (gray area under curve). A brisk-sustained cell distributes membrane as a narrow, steep Gaussian, so the same spot activates many synapses. A larger spot, filling the receptive field center, activates all synapses (cross-hatched), which are far more numerous for brisk cells (~6,000) than for local edge cells (~1,400).

There are other functional differences between ganglion cells that cannot be explained so simply. In particular, complex "trigger features," such as selectivity for direction-of-motion or a local edge, probably arise from specific amacrine circuits (Euler et al., 2002; Fried et al., 2002). Our studies do not contradict these observations. Rather, we emphasize the functional differences among ganglion cell types that result from differences in spatial concentration and extent of excitatory synapses.

LITERATURE CITED

Amthor FR, Oyster CW, Takahashi ES. 1984. Morphology of on-off direction-selective ganglion cells in the rabbit retina. Brain Res 298: 187–190.

Boots BN, Getis A. 1988. Point pattern analysis. Newbury Park, CA: Sage Publications. p 93.

Calkins D, Sterling P. 2007. Microcircuitry for two types of achromatic ganglion cell in primate fovea. J Neurosci 27:2646–2653.

Euler T, Detwiler PB, Denk W. 2002. Directionally selective calcium signals in dendrites of starburst amacrine cells. Nature 418:845–852.

Freed MA. 2000. Parallel cone bipolar pathways to a ganglion cell use

different rates and amplitudes of quantal excitation. J Neurosci 20: 3956–3963.

Freed MA, Sterling P. 1988. The ON-alpha ganglion cell of the cat retina and its presynaptic cell types. J Neurosci 8:2303–2320.

Freed MA, Smith RG, Sterling P. 1992. Computational model of the on-alpha ganglion cell receptive field based on bipolar cell circuitry. Proc Natl Acad Sci U S A 89:236–240.

Fried SI, Münch TA, Werblin FS. 2002. Mechanisms and circuitry underlying directional selectivity in the retina. Nature 420:411–414.

Haverkamp S, Wässle H. 2000. Immunocytochemical analysis of the mouse retina. J Comp Neurol 424:1–23.

Haverkamp S, Grünert U, Wässle H. 2000. The cone pedicle, a complex synapse in the retina. Neuron 27:85–95.

Jeon CJ, Kong JH, Strettoi E, Rockhill R, Stasheff SF, Masland RH. 2002. Pattern of synaptic excitation and inhibition upon direction-selective retinal ganglion cells. J Comp Neurol 449:195–205.

Jeong SA, Kwon OJ, Lee JY, Kim TJ, Jeon CJ. 2006. Synaptic pattern of AMPA receptor subtypes upon direction-selective retinal ganglion cells. Neurosci Res 56:427–434.

Jusuf PR, Martin PR, Grunert U. 2006. Synaptic connectivity in the midget-parvocellular pathway of primate central retina. J Comp Neurol 494:260–274.

Kier CK, Buchsbaum G, Sterling P. 1995. How retinal microcircuits scale for ganglion-cells of different size. J Neurosci 15:7673–7683.

Koch K, McLean J, Berry M, Sterling P, Balasubramanian V, Freed MA. 2004. Efficiency of information transmission by retinal ganglion cells. Curr Biol 14:1523–1530.

Koch K, McLean J, Segev R, Freed MA, Berry MJ 2nd, Balasubramanian V, Sterling P. 2006. How much the eye tells the brain. Curr Biol 16:1428–1434.

Kolb H. 1979. The inner plexiform layer in the retina of the cat: electron microscopic observations. J Neurocytol 8:295–329.

Kwon OJ, Kim MS, Kim TJ, Jeon CJ. 2007. Identification of synaptic pattern of kainate glutamate receptor subtypes on direction-selective retinal ganglion cells. Neurosci Res 58:255–264.

Lin B, Martin PR, Solomon SG, Grunert U. 2000. Distribution of glycine receptor subunits on primate retinal ganglion cells: a quantitative analysis. Eur J Neurosci 12:4155–4170.

Linsenmeier RA, Frishman LJ, Jakiela HG, Enroth-Cugell C. 1982. Receptive field properties of x and y cells in the cat retina derived from contrast sensitivity measurements. Vis Res 22:1173–1183.

Lorensen W, Cline H. 1987. Marching cubes: a high resolution 3D surface reconstruction algorithm. Comput Graphics 21:163–169.

McGuire BA, Stevens JK, Sterling P. 1986. Microcircuitry of beta ganglion cells in cat retina. J Neurosci 6:907–918.

Muresan V, Lyass A, Schnapp BJ. 1999. The kinesin motor KIF3A is a component of the presynaptic ribbon in vertebrate photoreceptors. J Neurosci 19:1027–1037.

Peichl L, Wässle H. 1981. Morphological identification of on- and off-centre brisk transient (Y) cells in the cat retina. Proc R Soc London B Biol Sci 212:139–153.

Robinson SR, Dreher Z. 1990. Muller cells in adult rabbit retinae: morphology, distribution and implications for function and development. J Comp Neurol 292:178–192.

Rockhill RL, Daly FJ, MacNeil MA, Brown SP, Masland RH. 2002. The diversity of ganglion cells in a mammalian retina. J Neurosci 22:3831–3843.

Roska B, Werblin F. 2001. Vertical interactions across ten parallel, stacked representations in the mammalian retina. Nature 410:583–587.

Singer JH, Lassova L, Vardi N, Diamond JS. 2004. Coordinated multivesicular release at a mammalian ribbon synapse. Nat Neurosci 7:826–833.

Sterling P, Matthews G. 2005. Structure and function of ribbon synapses. Trends Neurosci 28:20–29.

tom Dieck S, Altrock WD, Kessels MM, Qualmann B, Regus H, Brauner D, Fejtova A, Bracko O, Gundelfinger ED, Brandstatter JH. 2005. Molecular dissection of the photoreceptor ribbon synapse: physical interaction of Bassoon and RIBEYE is essential for the assembly of the ribbon complex. J Cell Biol 168:825–836.

Troy JB, Shou T. 2002. The receptive fields of cat retinal ganglion cells in physiological and pathological states: where we are after half a century of research. Prog Ret Eye Res 21:263–302.

Vaney DI. 1994. Territorial organization of direction-selective ganglion cells in rabbit retina. J Neurosci 14:6301–6316.

Vincent L, Soille P. 1991. Watersheds in digital spaces: an efficient algorithm based on immersion simulations. IEEE Transact Pattern Anal Machine Intel 13:583–598.

Weber AJ, Mccall MA, Stanford LR. 1991. Synaptic inputs to physiologically identified retinal x-cells in the cat. J Comp Neurol 314:350–366.

Xu Y, Dhingra NK, Smith RG, Sterling P. 2005. Sluggish and brisk ganglion cells detect contrast with similar sensitivity. J Neurophysiol 93:2388–2395.

Zhang LL, Fina ME, Vardi N. 2006. Regulation of KCC2 and NKCC during development: membrane insertion and differences between cell types. J Comp Neurol 499:132–143.

Zhang LL, Delpire E, Vardi N. 2007. NKCC1 does not accumulate chloride in developing retinal neurons. J Neurophysiol 98:266–277.